ELSEVIER

Journal of Organometallic Chemistry 655 (2002) 96–104

Journal of Organometallic Chemistry

www.elsevier.com/locate/jorganchem

Dimers of highly π-loaded organoimido d^1 metal radicals of niobium, tantalum, molybdenum, tungsten, and rhenium: the context of the cyclopentadienyl imido ligand analogy☆

Udo Radius [a], Andrea Schorm [b], Diane Kairies [c], Simone Schmidt [c], Frank Möller [c], Hans Pritzkow [d], Jörg Sundermeyer [b,*]

[a] *Institut für Anorganische Chemie der Universität Karlsruhe, Engesserstrasse, Geb. 30.45, 76128 Karlsruhe, Germany*
[b] *Fachbereich Chemie der Universität Marburg, Hans-Meerwein-Strasse, 35032 Marburg Lahn, Germany*
[c] *Institut für Anorganische Chemie der Universität Würzburg, Am Hubland, 97074 Würzburg, Germany*
[d] *Anorganisch-Chemisches Institut der Universität Heidelberg, Im Neuenheimer Feld 270, 69120 Heidelberg, Germany*

Received 3 January 2002; accepted 3 April 2002

Dedicated to Professor Walter Siebert on the occasion of his 65th birthday.

Abstract

The reductive generation and dimerisation of highly π-loaded and coordinatively unsaturated d^1 imido metal radicals of the type $[Cp_2M(NR)]$ (M = Nb, Ta), $[CpM(NR)_2]$ (M = Mo, W), and $[Re(NR)_3]$ is described. Their dinuclear spin-coupled complexes are characterized by crystal structure determinations and their bonding situation is discussed with reference to the cyclopentadienyl imido ligand analogy. © 2002 Elsevier Science B.V. All rights reserved.

Keywords: Imido complexes, organometallic; Niobium; Tantalum; Molybdenum; Tungsten; Rhenium; Metal–metal bonds

1. Introduction

The series of d^1 imido complex fragments of Group 5, 6, and 7 metals shown in Fig. 1 are related by the cyclopentadienyl imido ligand analogy [1–3]. They are formally obtained by homolytic cleavage of the M–Cl or M–C bonds at parent pseudotetrahedral d^0 imido metal chloro or alkyl complexes. As a common feature their number of occupied ligand orbitals of π-symmetry is larger than the number of empty metal d-orbitals available for π-interaction. Therefore, such complex fragments are termed π-loaded [4–6]. If, for example, these d^1 metal radicals are coupled with another C_5H_5 radical, it is σ- and not π-bonded. In the presence of other π-bound C_5H_5 groups within the ligand regime, a fluxional σ,π-exchange of cyclopentadienyl rings as well as the 1,5-metallotropic migration of the metal within the σ-bonded C_5H_5 ring is observed in the low temperature limiting NMR spectra of isolobally related $[Cp_4Zr]$ [7], $[Cp_3Nb(NR)]$ [8,9], $[Cp_3Ta(NR)]$ [9], $[Cp_2Mo(NR)_2]$ [10], $[Cp_2W(NR)_2]$ [10], and $[CpTc(NR)_3]$ [11].

The present study is concerned with the reductive generation and dimerisation of highly π-loaded and coordinatively unsaturated $4d^1$ and $5d^1$ radicals of Group 5–7 metals. Only a limited number of such dimers of the d^1 imido metal radicals has been described so far: Green et al. obtained the d^1 dimer *anti*-$[Cp'Mo(NPh)(\mu\text{-}NPh)]_2$ ($Cp' = MeC_5H_4$) by phenylisocyanate metathesis of corresponding d^1 oxo complexes [12,13]. The diamagnetic character has been attributed to spin coupling via a direct Mo–Mo interaction [12]. The corresponding d^1 rhenium imido dimer $[Re(N\textit{t}\text{-}Bu)_2(\mu\text{-}N\textit{t}\text{-}Bu)]_2$ with symmetrically bridging imido ligands was described by Wilkinson et al. [14] and the

☆ Part of a lecture given at the International Symposium of the SFB 247 'Interactions of π-Systems with Metals', Heidelberg, 26–28 April 2001.

* Corresponding author. Tel.: +49-6421-28-25693; fax: +49-6421-28-28917.
E-mail address: jsu@chemie.uni-marburg.de (J. Sundermeyer).

0022-328X/02/$ - see front matter
PII: S0022-328X(02)01423-7

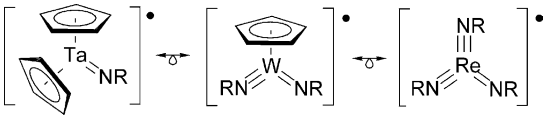

Fig. 1. Isolobal 17-VE d^1 metal radicals related by the cyclopentadienyl imido ligand analogy: The M–N bond order is determined by the maximum of 5 π-bonds per pseudo-tetrahedrally coordinated metal centre.

related aryl derivative $[Re(NDip)_3]_2$ (Dip = 2,6-*i*-$Pr_2C_6H_3$) with all terminal imido ligands and a non ligand supported Tc–Tc and Re–Re bond by Bryan et al. [15,16]. Isolobal $4d^1$ niobium and $5d^1$ tantalum complexes of the type $[Cp_2M(NR)]_2$ have not been investigated so far. However, it is known that $3d^1$ vanadocene imido complexes $[Cp_2V(NR)]$ do not tend to dimerize in the solid state or solution [17–22], they are stable as paramagnetic mononuclear species. Therefore, we set out to investigate the d^1 complex chemistry of the heavier Group 5 homologues and to compare it with isolobal relatives of Group 6 and 7.

2. Results and discussion

2.1. $4d^1$ Niobium and $5d^1$ tantalum imido complexes

Contrastingly to $3d^1$ vanadocenes, corresponding $4d^1$ niobocene and $5d^1$ tantalocene imido complexes are prone to form diamagnetic spin-coupled dimers **1** and **2**. Their synthesis is achieved by reduction of parent d^0 metal chloro complexes by Na/Hg or C_8K (Scheme 1). The dinuclear nature of **1** and **2** is in accord with the molecular ions found in the mass spectra. On the basis of 400 MHz ^{1}H-NMR spectra of yellow **1** or colourless **2** in temperature range $173 \leq T \geq 373$ K, a symmetrical structure with four chemically equivalent η^5-C_5H_5 ligands was initially proposed. However, in the low temperature limiting ^{1}H- and ^{13}C-NMR spectra a tendency of line broadening of the C_5H_5 signal was observed for both **1** and **2**.

In order to gain more insight into the bonding situation of these dimers, a crystal structure determination was carried out. Single crystals were obtained from a saturated solution of **2** in benzene–*n*-hexane. The molecular structure is shown in Fig. 2.

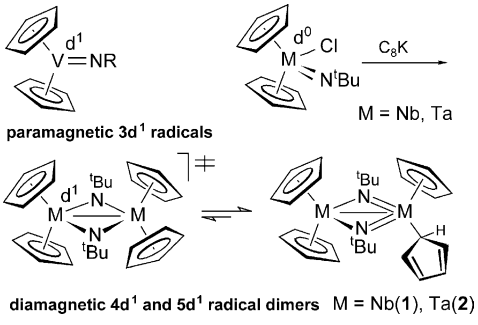

Scheme 1. Synthesis of d^1–d^1 niobocene and tantalocene imido complexes.

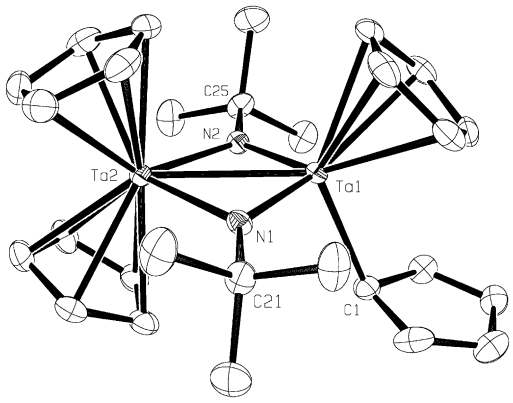

Fig. 2. Molecular structure of **2**. Selected bond distances (pm) and angles (°): Ta(1)–N(1) 190.7(5), Ta(1)–N(2) 193.0(5), Ta(2)–N(2) 213.9(5), Ta(2)–N(1) 214.4(5), Ta(1)–C(1) 235.4(7), Ta(1)–Ta(2) 283.82(8), N(1)–C(21) 150.8(8), N(2)–C(25) 152.6(8), C(1)–C(2) 145.4(11), C(1)–C(5) 146.6(10), C(2)–C(3) 133.9(12), C(3)–C(4) 143.6(11), C(4)–C(5) 135.3(10); N(1)–Ta(1)–N(2) 97.4(2), N(2)–Ta(2)–N(1) 84.7(2), Ta(1)–N(1)–Ta(2) 88.7(2), Ta(1)–N(2)–Ta(2) 88.3(2), N(1)–Ta(1)–C(1) 101.2(3), N(2)–Ta(1)–C(1) 99.7(2), N(1)–Ta(1)–Ta(2) 49.05(14), N(2)–Ta(1)–Ta(2) 48.9(2), C(1)–Ta(1)–Ta(2) 111.5(2), C(21)–N(1)–Ta(1) 138.7(4), C(21)–N(1)–Ta(2) 132.6(4), C(25)–N(2)–Ta(1) 136.9(4), C(25)–N(2)–Ta(2) 134.4(4).

We were surprised to learn that in the solid state three cyclopentadienyl ligands are η^5- and one cyclopentadienyl ligand is η^1-bonded. As a consequence the imido ligands are asymmetrically bridging both tantalum atoms. The two short Ta–N bonds are observed at Ta1 binding only one η^5-C_5H_5 ring as π-donor and the two long Ta–N bonds are observed at Ta2 with two π-donor ligands η^5-C_5H_5. It seems that the formation of two strong Ta–N π-bonds within the planar Ta_2N_2 ring is responsible for pushing one of the four C_5H_5 rings out of π-coordination. The loss of two π-bonds to C_5H_5 is compensated by two new π-bonds to the asymmetrically bridging nitrogen atoms. The asymmetric polarisation of the molecule discloses some character of a contact ion pair $[(\eta^5\text{-}C_5H_5)_2Ta]^{2+}[(NR)_2Ta(\eta^5\text{-}C_5H_5)(\eta^1\text{-}C_5H_5)]^{2-}$. If we accept that the asymmetric structure is not the result of steric ligand congestion, it can be concluded, that the bridging 2σ, 1π-donor $[NR]^{2-}$ forms a stronger π-bond with a highvalent d^1 tantalum centre than a $[\eta^5\text{-}C_5H_5]^-$ ligand revealing more diffuse and polarizable π-orbitals (e_2 set of group orbitals). The coupling of the spins at tantalum may be interpreted via a direct metal–metal orbital interaction [12] or by super exchange [14] via the bridging ligand orbitals. According to Wilkinson et al. [14] four-membered $[M_2(\mu\text{-}NR)_2]$ cores should have a direct M–M bonding interaction, when M–N–M angles are in the range of 78–84° and they should have no direct M–M interaction, when angles are >94°. In **2**, the Ta–Ta distance of 283.82(8)

pm and the Ta–N–Ta angles 88.7(2) and 88.3(2) indicate a weak Ta–Ta bonding interaction. In related but not π-bond saturated diamagnetic d^1–d^1 complexes $[(\eta^5\text{-}C_5H_5)M(\mu\text{-}Nt\text{-}Bu)Cl]_2$ (M = Nb, Ta) [23] no fluxional ligand rearrangements are observed.

2.2. $4d^1$ Molybdenum and $5d^1$ tungsten imido complexes

Dimers of isolobally related π-bond saturated d^1 radicals $[CpM(NR)_2]$ (M = Mo, W) can be synthesized by reduction of d^0 complexes $[CpM(NR)_2Cl]$ (M = Mo, W, R = *t*-Bu, Mes) with Na/Hg or C_8K (Scheme 2).

The synthesis of the starting material $[CpW(NMes)_2Cl]$ (**3**) follows the strategy outlined before [24–26]. In all cases of reductive generation and coupling of the d^1 molybdenum and tungsten radicals we observe two sets of NMR signals of diamagnetic products indicating the formation of *syn*- and *anti*-isomers in different ratios. The ratio of isomers did not change, when NMR samples were heated at 140 °C for several hours. Solutions of pure *syn*- or *anti*-isomers did not isomerise under these conditions, indicating that these products are formed under kinetic control via non-reversible dimerisation of d^1 metal radicals. This is in contrast to *anti*-$[(\eta^5\text{-}C_5H_4Me)Mo(NPh)(\mu\text{-}NPh)]_2$ that has been synthesized via phenyl isocyanate metathesis at corresponding d^1 oxo complexes [12]. Under these reaction conditions of thermodynamic control only the *anti*-isomers were spectroscopically observed and structurally characterized. However, there is a report of Wiberg et al. that oxidative addition of bis-trimethylsilyl diazene at chromocene leads to *cis*-$[(\eta^5\text{-}C_5H_5)Cr(NSiMe_3)(\mu\text{-}NSiMe_3)]_2$ [27], probably the product of kinetic reaction control. In order to assign the signals of our major products to the predominant stereoisomers, we set out to determine crystal structures of representative examples of d^1–d^1 dimers. Figs. 3 and 4 show the result of two crystal structure determinations. They reveal the trend, that the major products of a kinetically controlled irreversible dimerisation of d^1 species $[(\eta^5\text{-}C_5R_5)Mo(NR)_2]$ generated at the surface of the reductants are in fact *syn*-dimers. The isomer ratios have been

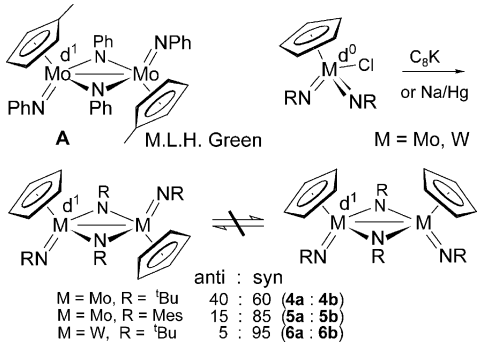

Scheme 2. Synthesis of d^1–d^1 molybdenum and tungsten imido complexes.

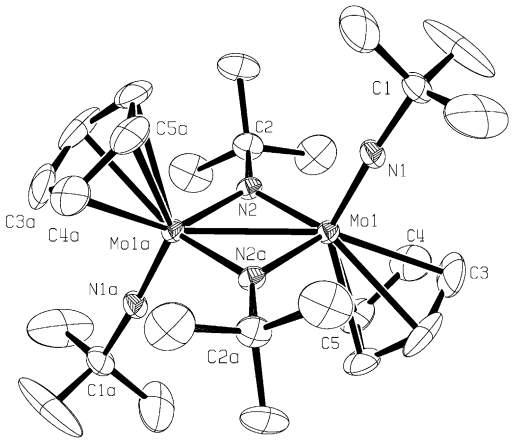

Fig. 3. Molecular structure of **4a**. Selected bond distances (pm) and angles (°): Mo(1)–N(1) 173.5(6), Mo(1)–N(2) 196.2(4), Mo(1)–C(3) 240.8(11), Mo(1)–C(4) 242.8(7), Mo(1)–C(5) 251.3(6), Mo(1)–Mo(1a) 270.67(12), N(1)–C(1) 144.4(9), N(2)–C(2) 149.1(9); N(1)–Mo(1)–N(2) 105.79(14), Mo(1)–N(2)–Mo(1a) 87.2(2), N(2)–Mo(1)–N(2a) 92.8(2), N(1)–Mo(1)–Mo(1a) 113.2(2), Mo(1)–N(1)–C(1) 175.9(6), Mo(1)–N(2)–C(2) 136.40(11).

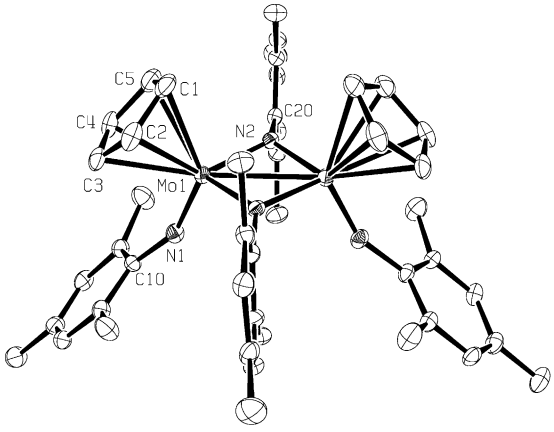

Fig. 4. Molecular structure of **5b**. Selected bond distances (pm) and angles (°); X is the centroid of the Cp ligand C(1)–C(5): Mo(1)–N(1) 178.0(3), Mo(1)–X 209.4, Mo(1)–N(2) 198.7(3), Mo(1)–C(1) 240.1(5), Mo(1)–N(2a) 197.2(4), Mo(1)–C(2) 239.6(5), Mo(1)–Mo(1a) 277.2(1), Mo(1)–C(3) 241.9(4), N(1)–C(10) 139.4(5), Mo(1)–C(4) 242.4(5), N(2)–C(20) 141.9(6) Mo(1)–C(5) 240.7(5); Mo(1)–N(2)–Mo(1a) 88.88(15), N(1)–Mo(1)–N(2) 108.42(14), N(1)–Mo(1)–N(2a) 109.18(16), Mo(1)–N(1)–C(10) 154.7(3), N(2)–Mo(1)–N(2a) 90.97(15), Mo(1)–N(2)–C(20) 132.4(3).

determined from the ^{1}H-NMR integrals of the crude reaction mixture and the assignment to stereoisomers was accomplished by comparison of NMR spectra of separated pure crystals that were submitted to X-ray analyses. For R = *tert*-butyl, the minor *anti*-isomer **4a** was used for the crystallographic work, for R = mesityl, the major *syn*-isomer **5b**.

Greenish–yellow single crystals of **4a** were obtained by slow evaporation of a saturated *n*-hexane solution of the mixture of isomers **4a**, **b**. The molecule **4a** reveals crystallographically imposed C_{2h} symmetry with a

Table 1
Selected structural parameters of *anti*-[CpMo(N*t*-Bu)(μ-N*t*-Bu)]$_2$ (**4a**), *syn*-[CpMo(NMes)(μ-NMes)]$_2$ (**5b**) and *anti*-[(η^5-C$_5$H$_4$Me)Mo(NPh)(μ-NPh)]$_2$ (**A**)

	Mo–Mo (pm)	Mo–N$_{term.}$ (pm)	Mo–N$_{br.}$ (pm)	Mo–N–Mo (°)
4a	270.67(12)	174.4(8)	196.3(8)	87.2(3)
5b	277.2(1)	178.0(3)	198.7(3)	88.88(15)
			197.2(4)	
A [12]	271.75(5)	176.3(3)	197.5(2)	92.8(1)
			196.4(2)	

centre of inversion in the middle of the planar inner [Mo$_2$(μ-NR)$_2$] core (Fig. 3). Consequently the imido ligands are symmetrically bridging. A comparison of selected bonding distances with **5b** and the literature-known complex **A** of this class is presented in Table 1.

In a similar way red crystals of *syn*-**5b** were obtained next to a yellow precipitate of *anti*-**5a** from a saturated solution of **5a**, **b** in *n*-hexane. Fig. 4 displays the result of the crystal structure analysis. The asymmetric unit contains half the molecule, the other half of **5b** is obtained by applying a σ- and C_2-symmetry operation. Thus an edge-bridged tetrahedral configuration for each molybdenum atom with close to symmetrically bridging imido ligands and an almost planar [Mo$_2$(μ-NR)$_2$] ring are observed. The bonding distance Mo(1)–Mo(1a) of *syn*-[CpMo(NMes)(μ-NMes)]$_2$ (**5b**) is considerably longer than in *anti*-[(η^5-C$_5$H$_4$Me)Mo(NPh)(η-NPh)]$_2$ and in *anti*-[(η^5-C$_5$H$_5$)Mo(N*t*-Bu)(μ-N*t*-Bu)]$_2$ (**4a**), but short enough for d^1–d^1 spin-coupling. Further selected structural parameters are compared in Table 1.

The question arises whether dimerisation and spin coupling may be inhibited by sterically more demanding ligands. In a first effort to follow this strategy the reduction of [Cp*Mo(N*t*-Bu)$_2$Cl] with C$_8$K in toluene was tested. However, this reaction afforded a dinuclear, spin-coupled d^1–d^1 dimer **7**. An absolute reliable assignment to either a *syn*- or *anti*-configuration of **7** cannot be made without having structural data available. We assume, however, that the only isomer observed corresponds to a *syn*-structure. This is in accord with our mechanistic proposal, that dimerisation is favourably accomplished by surface-bound d^1 metal radicals (Scheme 3), especially when non-co-ordinating solvents such as toluene are used.

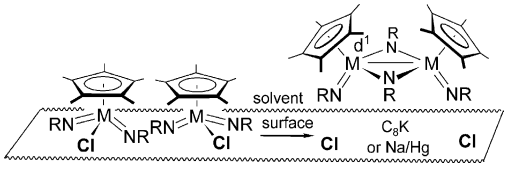

Scheme 3. Proposal for reduction and dimerisation as a surface reaction: preferential formation of *syn*-isomers.

As we never observed a *syn*-/*anti*-isomerisation of the isolated imido bridged isomers in solution, the most reasonable pathway to *anti*-isomers may best be accomplished after solvation and dissociation of the coordinatively unsaturated d^1 metal radicals from the reductant surface. In this respect it is interesting to note, that reduction of related [Cp*W(NMes)$_2$Cl] with C$_8$K in THF, a good ligand and potential source of H radicals, leads to the isolation of the hydrido complex [Cp*W(NMes)$_2$H] as the trapped d^1 metal radical [28].

2.3. 5d^1 Rhenium imido complexes

The isolobally related d^1–d^1 complexes of the type [Re(NR)$_3$]$_2$ have already been the focus of recent investigations [14,15]. For R = *t*-Bu, Wilkinson et al. described a dinuclear rhenium complex with symmetrically bridging imido ligands [14] whereas for sterically more demanding N-aryl ligands, R = 2,6-diisopropylphenyl (Dip), Bryan et al. reported a d^1–d^1 dimer with a non-ligand-supported Re–Re bond and only terminal imido ligands [15]. There is evidence that this fascinating difference in bonding is a consequence of steric and not electronic influence of the N-substituent [16]. In order to gain insight into this problem, we have synthesized and structurally characterized the sterically less demanding mesityl imido complex **10** (Scheme 4).

The synthesis of **10** is accomplished in three steps: (1) conversion of [Re$_2$O$_7$] into the imido silylester **8** of rhenic acid following the method outlined for related [Re(N*t*-Bu)$_3$OSiMe$_3$] [29], (2) converting **8** into the imido rhenic acid chloride **9** by treatment with TMSCl and (3) reduction of **9** by C$_8$K in toluene. However, better yields of **10** were obtained by reaction of **9** with Li[HBEt$_3$] in THF at −78 °C. Upon slow warming to room temperature, orange **10** precipitates from the reaction mixture. It is interesting to note that the proposed intermediate [Re(NMes)$_3$H] [30], which could not be detected at our reaction conditions, seems to be unstable with respect to loss of dihydrogen and forma-

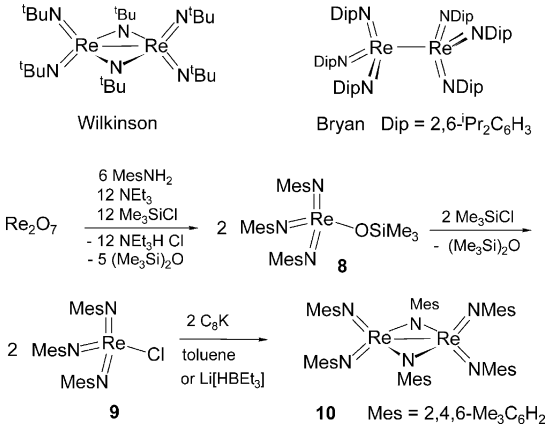

Scheme 4. Synthesis of the d^1–d^1 rhenium imido complex **10**.

tion of **10**, while [Re(NDip)$_3$H] is thermodynamically stable and kinetically inert with respect to loss of H_2 [31]. The ^{1}H-NMR spectrum of **10** reveals four signals for chemically equivalent methyl protons: 24H for terminal *ortho*-CH_3 groups, 12H for terminal *para*-CH_3 groups, 12H for bridging *ortho*-CH_3 groups, and 6H for bridging *ortho*-CH_3 groups. By applying vt-NMR experiments in toluene-d_8 in the range 193–373 K, we have no clear evidence for an exchange of terminal and bridging imido ligands or for a second stable isomer with all-terminal imido ligands. In order to gain more insight into the nature of the bridging ligand mode, single crystals of **10** were grown from a saturated THF solution. The result of the crystal structure analysis is shown in Fig. 5.

The molecule is build up from two edge-sharing [ReN_4] tetrahedra. It reveals a crystallographically imposed C_2 axis defined by the vector N(3)–N(3a) of the planar [$Re_2(\mu\text{-}NR)_2$] ring and a crystallographic inversion center located at the midpoint of the Re–Re bond similar to the Tc–Tc homologue with *ortho*-xylyl imido ligands [15]. The distances Re(1)–N(3) 194.8(5) pm and Re(1)–N(3a) 195.3(4) of the four-membered ring are close to identical within the limits of accuracy of measurement, however, the bonding distances to the terminal imido ligands Re(1)–N(1) 174.5(5) and Re(1)–N(2) 176.1(5) pm are significantly shorter. The Re(1)–Re(1a) distance 272.7(1) pm is considerably longer than 270 pm found in [Re(N*t*-Bu)$_2$(μ-N*t*-Bu)]$_2$ [14]. Refinement data of this previously reported homoleptic d^1–d^1 imido complex are of poor quality, therefore, only

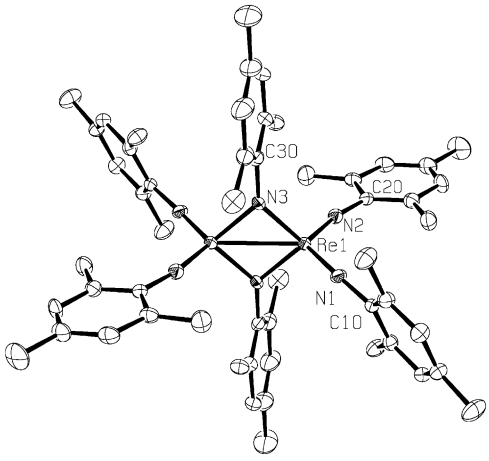

Fig. 5. Molecular structure of **10**. Selected bond distances (pm) and angles (°): Re(1)–N(1) 174.5(5), N(1)–C(10) 139.1(7), Re(1)–N(2) 176.1(5), N(2)–C(20) 137.7(7), Re(1)–N(3) 194.8(5), N(3)–C(30) 142.6(7), Re(1)–N(3a) 195.3(4), Re(1)–Re(1a) 272.7(1); Re(1)–N(3)–Re(1a) 88.70(19), Re(1)–N(1)–C(10) 167.0(4), N(3)–Re(1)–N3a) 91.30(19), Re(1)–N(2)–C(20) 167.6(4), N(1)–Re(1)–N(2) 114.1(2), Re(1)–N(3)–C(30) 138.3(4), N(1)–Re(1)–N(3) 114.3(2), N(1)–Re(1)-Re(1a) 122.37(16), N(2)–Re(1)–N(3) 113.1(2), N(2)–Re(1)–Re(1a) 123.39(16), N(1)–Re(1)–N(3a) 109.7(2), N(3)–Re(1)–Re(1a) 45.73(13).

average values for the distances Re–N(bridging) 191 pm and Re–N(terminal) 174 pm were given. The trend of longer Re–Re and Re–N distances in our complex **10** reflects the weaker donor capability of [NMes] versus [N*t*-Bu] ligands.

2.4. The question of valence electron-count and π-bond order

In complexes with a tetrahedral or pseudotetrahedral regime of four σ,2π-donor ligands such as [η^5-C_5R_5]$^-$ or [RN]$^{2-}$, symmetry restrictions in metal ligand orbital interactions are allowing a maximum of five π-bonds: two strong π-bonds by the e set, three weaker π-bonds by the t_2 set of metal d-orbitals being involved in both, σ- and π-bonding [1,32]. Because of the limited set of metal d-orbitals available, some electron density has to remain in non-bonding ligand centered orbitals if the four ligands offer more orbitals of π-symmetry than five [1,33]. This bonding situation is typical for highly π-bond loaded ligand regimes at the limit of π-bond saturation [4,5]. It is interesting to note that four σ-bonding and five π-bonding electron pairs add up to a 18-valence-electron shell for covalent molecules such as osmium tetroxide, or the organometallic species discussed here having an unsymmetrical five π-bond skeleton to four ligands of different π-donor capability. The question arises, which σ, 2π-donor is the strongest? In general crystallographic data do not allow a clear-cut classification as an imido ligand leads to an elongation of the M–C_5H_5 bonds especially in *trans*-position to NR, and one or two η^5-C_5H_5 ligands reduce considerably the M–N bond order of an imido ligand. If the variable π-electron donating ability of imido and cyclopentadienyl ligands and the maximum number of five π-bonds is taken into account, the d^1 complex fragments of Fig. 1 can be regarded as 17-valence electron (VE) species with different average M–N bond orders. We have proven that these 17-VE imido complex fragments form stable hetero-dinuclear and hetero-trinuclear complexes with typical 17-VE carbonyl complex fragments. The heteroleptic carbonyl imido complexes have M–M′ bonds without bridging ligands [3,34]. The present study summarizes our results on homo-dimerisation of these 17-VE imido complex fragments. In contrast to homo-dimers of 17-VE carbonyl complex fragments, which show extensive exchange of bridging and terminal carbonyl ligands, there is a strong preference for configuratively stable and non-fluxional homo-dimers with bridging imido ligands.

3. Experimental

The following d^0 metal imido complexes were obtained via published procedures: [Cp_2Nb(N*t*-Bu)Cl]

[23], [$Cp_2Ta(N$*t*-Bu)Cl] [23], [$CpMo(N$*t*-$Bu)_2Cl$] [24], [$CpW(N$*t*-$Bu)_2Cl$] [24] and [$Cp^*Mo(N$*t*-$Bu)_2Cl$] [26]. The synthesis of the corresponding mesitylimido complexes [$CpMo(NMes)_2Cl$] follows the route outlined in [24] starting with [$Mo(NMes)_2Cl_2$(dme)] [35], the synthesis of [$Re(NMes)_3Cl$] follows the route outlined for organoimido rhenium complexes with R = *tert*-butyl and 2,6-diisopropylphenyl [31]. The procedures for new starting materials are given below.

3.1. Synthesis of [$Cp_2Nb(\mu$-*Nt*-*Bu*)]$_2$ (**1**)

A mixture of 264 mg (0.80 mmol) [$Cp_2Nb(N$*t*-Bu)Cl] and 3.47 g (1.20 mmol) Na/Hg (0.95% Na) in 10 ml THF is stirred for 2 days at room temperature (r.t.). The solution is then separated via a cannula, filtered via a bed of Celite and the solvent is removed in vacuo. The residue is crystallized at 8 °C from C_6H_6. Yield: 367 mg (78%), orange solid, m.p. 212 °C.

^{1}H-NMR (200 MHz, C_6H_6-d_6): 1.11 (s, 18H), 5.63 (s, 20H). ^{13}C-NMR (50 MHz, C_6H_6-d_6) $\delta = 32.8$, 66.0, 100.9 ppm. ^{1}H-NMR (400 MHz, toluene-d_8, 200 K): 1.09 (s, br, 18H), 5.67 (s, br 20H) ppm. ^{13}C-NMR (100 MHz, toluene-d_8, 200 K): 32.7, 66.1, 100.8 ppm. IR (Nujol): 3096 w, 3080 w ν(C–H_{ar}), 1348 m, 1244 s and 1208 m ν(Nb–N–C), 1124 w, 1064 w, 1012 m, 840 m, 792 s δ(C–H_{ar})$_{oop}$. EIMS: $m/z = 588$ ($[M]^+$, 5%), 223 (1/2 $[M]^+$–$NC(CH_3)_3$, 100%). Anal. Found: C, 57.02; H, 6.45; N, 4.59. Calc. for $C_{28}H_{38}N_2Nb_2$ (588.43): C, 57.15; H, 6.51; N, 4.76%.

3.2. Synthesis of [$Cp_2Ta(\mu$-*Nt*-*Bu*)]$_2$ (**2**)

[(η^5-$C_5H_5)_2Ta(N$*t*-Bu)Cl] (150 mg, 0.36 mmol) and 75 mg (0.55 mmol) C_8K are suspended in 10 ml toluene and the mixture is treated for 12 h at 45 °C with ultrasound. The soluble parts are separated by filtration via celite, volatiles are removed at 40 °C per 10^{-2} mbar and the oily residue is washed with some ultrasonic support by 3×5 ml *n*-hexane at 0 °C. The soluble parts contain starting material, insoluble parts are collected and crystallized from benzene–*n*-hexane 2:1. At 5 °C colorless crystals were obtained. Yield: 206 mg (75%), crystalline colorless solid, m.p. 200 °C. ^{1}H-NMR (400 MHz, C_6H_6-d_6): 1.58 (s, 18H), 5.13 (s, 20H). ^{13}C-NMR (100 MHz, C_6H_6-d_6): 36.7, 64.9, 104.7. IR (Nujol): 3095 w ν(C–H_{ar}), 1353 m, 1170 s, 1017 m, 1009 m, 977 m, 969 m, 908 w, 836 m, 811 s δ(C–H_{ar})$_{oop}$, 787 m, 759 m, 707 s. EIMS: $m/z = 764$ ($[M]^+$, 18%), 707 ($[M]^+$–C_4H_9, 63%), 642 ($[M]^+$–C_5H_5–C_4H_9, 100%), 569 ($[M]^+$–$3C_5H_5$, 45%), 65 ($[C_5H_5]^+$, 40%), 57 ($[C_4H_9]^+$, 27%), 41 ($[C_3H_5]^+$, 58%). Anal. Found: C, 43.65; H, 4.74; N, 3.38. Calc. for $C_{28}H_{38}N_2Ta_2$ (764.52) C, 43.99; H, 5.01; N, 3.66%.

3.3. Crystal structure determination of **2**

Compound **2** crystallizes in the monoclinic space group $P2_1$ (No. 4) with $a = 9.709(3)$, $b = 8.532(1)$, $c = 15.062(5)$ Å, $\alpha = 90°$, $\beta = 98.71(1)°$, $\gamma = 90°$, $V = 1233(1)$ Å^3, $Z = 2$. A crystal with the dimensions $0.2 \times 0.1 \times 0.1$ mm^3 was used. Intensity data were measured at 298 K with a Enraf–Nonius CAD4 diffractometer (Mo–K_α radiation, $\lambda = 0.71073$ Å, ω-scans) up to $\Theta_{max} = 23°$, yielding 3161 unique reflections, of which 3007 were observed for index [$F_0 > 3\sigma(F_0)$]. The structure was solved by direct methods (SHELXS-86 and SHELXS-97) [36] and refined [37] by full-matrix least-squares methods (ENRAF–NONIUS SDP) to $R = 0.0177$, $wR_2 = 0.0203$; L/P correction, empirical absorption correction (Ψ-scan method, min. transmission 63.4%); residual electron density 0.652 e Å^{-3}. Non-hydrogen atoms were refined anisotropically, hydrogen atoms were inserted in calculated positions.

3.4. Synthesis of [$CpMo(NMes)_2Cl$] (**3**)

C_5H_5Li (72.0 mg, 1.00 mmol) dissolved in 50 ml Et_2O are added at −78 °C to 500 mg (0.96 mmol) [$Mo(NMes)_2Cl_2$(dme)]. Within 30 min the reaction mixture is allowed to reach r.t. After 2 h at r.t. all volatiles are removed in vacuo, the residue is extracted with 15 ml toluene and insoluble material is removed by filtration. Most of the toluene is evaporated and the product is precipitated by addition of 15 ml hexane. Yield: 333 mg (75%), dark red solid, m.p. 101 °C. ^{1}H-NMR (200 MHz, $CHCl_3$-*d*): 2.29 (s, 18H), 6.48 (s, 5H), 6.79 (s, 4H) ppm. ^{13}C-NMR (50 MHz, $CHCl_3$-*d*): 18.8, 20.9, 110.2, 128.1, 130.9, 135.0, 155.4 ppm. IR (Nujol): 3104 m ν(C–H_{ar}), 1600 m ν(C=C), 1320 vs and 1276 s ν(Mo=N–C), 1160 w, 1104 w, 1064 w, 1036 w, 1016 w, 976 m, 932 m, 868 m, 800 s ν(C–H_{ar})$_{oop}$, 724 m, 596 w, 560 w, 492 w, 456 m, 424 m cm^{-1}. EIMS: $m/z = 464$ ($[M]^+$, 100%), 429 ($[M]^+$–Cl, 18%), 331 ($[M]^+$–$C_9H_{11}N$, 83%). Anal. Found: C, 59.41; H, 5.91, N, 5.91. Calc. for $C_{23}H_{27}ClMoN_2$ (462.9): C, 59.68; H, 5.88; N, 6.05%.

3.5. Synthesis of anti-, syn-[$CpMo(N$*t*-*Bu*)(μ-*Nt*-*Bu*)]$_2$ (**4a**, **b**)

Na/Hg (2.08 g, 0.87 mmol) (0.95% Na) and 146 mg (0.43 mmol) [$CpMo(N$*t*-$Bu)_2Cl$] dissolved in 10 ml toluene are stirred at r.t. for 24 h. Soluble parts are separated, volatiles completely removed. The brown residue is extracted with 2×25 *n*-hexane at 55 °C, the combined yellow–brown extracts are filtered via celite and reduced in volume and set aside at −30 °C. A precipitate of greenish–yellow microcrystalline solid (*syn*-isomer) and yellow prisms (*anti*-isomer) *syn*/*anti* = 60/40 is collected. The ratio of isomers did not change after a second recrystallisation from hexane.

Yield: 102 mg (78%) mixture of isomers, dec. > 202 °C. ^{1}H-NMR (90 MHz; C_6H_6-d_6) *syn*-isomer: 0.96 (s, 18H), 1.75 (s, 18H), 5.69 (s, 10H); *anti*-isomer: 0.89 (s, 18H), 1.82 (s, 18H), 5.79 (s, 10H). ^{13}C-NMR (100 MHz, C_6H_6-d_6) *syn*-isomer: 31.5, 35.7, 66.2, 67.9, 101.8; *trans*-isomer: 31.2, 35.5, 67.6, 68.6, 102.4 ppm. IR (Nujol) mixture of isomers: 3098 w ν(C–H_{ar}), 1228 vs and 1184 s ν(Mo=N–C), 1132 vw, 1012 m, 844 w, 795 s ν(C–H_{ar})$_{oop}$, 656 vw, 608 vw, 572 vw, 520 m cm^{-1}. IR (Nujol) *anti*-isomer: 3092 w ν(C–H_{ar}), 1236 vs and 1180 s ν(Mo=N–C), 1100 vw, 1008 m, 844 w, 804 s, 780 s ν(C–H_{ar})$_{oop}$, 724 w, 660 w, 612 w, 568 vw, 524 m cm^{-1}. EIMS: $m/z = 606$ ([M]$^+$, 16%), 591 ([M]$^+$–CH_3, 100%), 534 ([M]$^+$–CH_3–C_4H_9, 6%). Anal. Found: C, 51.43, H, 7.63; N, 9.17. Calc. for $C_{26}H_{46}Mo_2N_4$ (606.6): C, 51.49; H, 7.64; N: 9.24%.

3.6. Crystal structure determination of **4a**

Compound **4a** crystallizes in the orthorhombic space group *Cmca* with $a = 11.155(8)$, $b = 17.774(16)$, $c = 14.807(11)$ Å, $V = 2936(2)$ Å^3, $Z = 4$. A crystal with the dimensions $0.34 \times 0.30 \times 0.07$ mm^3 was used. Intensity data were measured at r.t. with a Siemens–Stoe AED2 diffractometer (Mo–K_α radiation, $\lambda = 0.71073$ Å, ω-scans) up to $\Theta_{max} = 27°$, yielding 1695 unique reflections, of which 980 were observed with $I > 2\sigma(I)$. The structure was solved by direct methods (SHELXS-86, SHELXS-97) [36] and refined [37] by least-squares methods based on F^2 with all reflections to $R_1 = 0.044$ (observed reflections only) and $wR_2 = 0.1136$ (all reflections), residual electron density 0.43/−0.75 e Å^{-3}. Non-hydrogen atoms were refined anisotropically, hydrogen atoms were inserted in calculated positions. The *tert*-butyl groups of the bridging imido ligands are disordered, one of the two positions is shown.

3.7. Synthesis of anti-, syn-[CpMo(NMes)(μ-NMes)]$_2$ (**5a**, **b**)

C_8K (80 mg, 0.594 mmol) are added to a solution of 250 mg (0.540 mmol) [(η^5-C_5H_5)Mo(NMes)$_2$Cl] in 20 ml THF. The suspension is stirred at r.t. for 22 h, volatiles are removed in vacuo, the product is extracted into 50 ml *n*-hexane, graphite and other insoluble materials are separated by filtration via celite and the solution is kept at −30 °C. An precipitate of red crystals (*syn*-isomer) and a yellow microcrystalline solid (*anti*-isomer) *syn*/*anti* = 82/18 is collected. Yield mixture of isomers: 200 mg (47%), dec. > 198 °C. ^{1}H-NMR (200.13 MHz, C6H6-d_6): *syn*-isomer: 2.05 (s, br, 6H), 2.07 (s, br, 12H), 2.13 (s, br, 6H), 2.19 (s, br, 12H), 5.67 (s, 10H), 6.63 (s, 4H), 6.92 (s, 2H), 7.07 (s, 2 H); *anti*-isomer 2.31 (s, br, 6H), 2.32 (s, br, 24H), 2.34 (s, br, 6H), 5.61 (s, 10H), 6.73 (s, 4H), 6.77 (s, 2H), 6.97 (s, 2H) ppm. ^{13}C-NMR (100 MHz, C6H6-d_6): *syn*-isomer: 20.1, 20.8, 21.0, 21.9, 105.5, 128.9, 129.2, 130.0, 130.2, 131.9, 132.9, 150.4, 165.6 ppm; *anti*-isomer: Due to the low content of *anti*-isomer, a full set of ^{13}C-NMR signals was not obtained. IR (Nujol): 1636 w ν(C=C), 1375 s, 1341 vs, 1294 m and 1249 vs ν(Mo=N–C), 1231 m, 1224 w, 1163 m, 1092 vw, br, 1020 s, 1015 w, 959 m, 913 s, 878vs, 847 vsm 816 vsm 796 vs, 670 m, 622 w, 586 w cm^{-1}. EIMS: $m/z = 855$ ([M]$^+$, 100%), 789 ([M]$^+$–Cp, 43%), 721 ([M]$^+$–NMes, 59%), 427 ([CpMo(NMes)$_2$], 74%). Anal. Found: C, 64.63, H, 6.37; N, 6.55. Calc. for $C_{46}H_{54}Mo_2N_4$ (854.84): C, 64.16; H, 5.94, N, 6.25%.

3.8. Crystal structure determination of **5b**

Compound **5b** crystallizes in the monoclinic space group *C*2/*c* (No. 5) with $a = 22.716(7)$, $b = 8.650(4)$, $c = 21.099(3)$ Å, $\alpha = \gamma = 90°$, $\beta = 105.04(4)°$, $V = 4004(2)$ Å^3, $Z = 4$. A crystal with the dimensions $0.3 \times 0.2 \times 0.1$ mm^3 was used. Intensity data were measured at 223 K with a Siemens P4 diffractometer (Mo–K_α radiation, $\lambda = 0.71073$ Å) upto $\Theta_{max} = 25°$, yielding 2689 unique reflections, of which 2100 were observed. The absorption coefficient was 0.663 mm^{-1}, no absorption correction. The structure was solved by direct methods (SHELXS-86, SHELXS-97) [36] and refined [37] by least-squares methods based on F_2 with all reflections to $R = 0.0296$ and $wR_2 = 0.1039$; residual electron density 0.330/−0.380 e Å^{-3}. Non-hydrogen atoms were refined anisotropically, hydrogen atoms were inserted in calculated positions.

3.9. Synthesis of anti-, syn-[CpW(Nt-Bu)(μ-Nt-Bu)]$_2$ (**6a**, **b**)

C_8K (150 mg, 1.11 mmol) are added to a solution of 300 mg (0.703 mmol) [CpW(N*t*-Bu)$_2$Cl] in 10 ml THF. After stirring for 20 h at r.t. and removing the solvent in vacuo, the product is extracted into 10 ml hexane. Solids are separated by filtration via celite and part of the solvent is evaporated. A light yellow microcrystalline precipitate containing 95% *syn*-isomer and 5% *anti*-isomer (NMR) is collected. Yield: 215 mg (78%), dec. > 214 °C. ^{1}H-NMR (400 MHz, C_6H_6-d_6): *syn*-isomer: 0.92 (s, 18H), 1.80 (s, 18H), 5.81 (s, 10H), *anti*-isomer: 1.02 (s, 18H), 1.75 (s, 18H), 5.65 (s, 10H) ppm. ^{13}C-NMR (100 MHz, C_6H_6-d_6): *syn*-isomer: 101.3, 69.2, 65.9, 35.8, 32.1; *anti*-isomer: 100.4, 36.0, 32.2 ppm. IR (Nujol): 1455 vs, sh, 1376 s, 1355 m and 1270 m ν(W=N–C), 1201 vw, 1179 m, 1080 vw, 1008 w, 888 vw, 841 vw, 805 m, 781 m, 718 vw, 603 vw, 525 vw cm^{-1}. EIMS: $m/z = 782.4$ ([M]$^+$, 63%), 767.3 ([M]$^+$–CH_3, 60%), 725.3 ([M]$^+$–C_4H_9, 100%). Anal. Found: C, 39.48; H, 5.67; N, 6.42. Calc. for $C_{26}H_{46}N_4W_2$ (782.4): C, 39.92; H, 5.93; N, 7.16%.

3.10. Synthesis of [Cp*Mo(Nt-Bu)(μ-Nt-Bu)]$_2$ (7)

C_8K (150 mg, 1.11 mmol) are added to a solution of 300 mg (0.73 mmol) [Cp*Mo(N*t*-Bu)$_2$Cl] in 40 ml toluene and the suspension is treated with ultrasound for 90 min. Insoluble parts are separated by filtration via celite. Volatiles of the filtrate are completely removed in vacuo and the orange–brown residue is crystallized from *n*-pentane at −80 °C. Yield: 102 mg (82%) orange crystals, m.p. 103 °C. ^{1}H-NMR (200 MHz, C_6H_6-d_6), only one isomer detectable: 1.11 (s, 9H), 1.90 (s, 9H), 1.98 (s, 15H). ^{13}C-NMR (50 MHz, C_6H_6-d_6): 14.4, 33.2, 33.9, 66.3, 69.3, 114.3 ppm. IR (Nujol): 1208 vs and 1176 s ν(Mo=N–C), 1112 m, 1020 m, 968 m, 912 w, 804 w, 752 vw, 720 w, 685 vw, 620 sh, 556 w, 516 m, 492 w, 460 w, 424 w cm^{-1}. EIMS: $m/z = 746$ ([M]$^+$, 13%), 611 ([M]$^+$–$C_{10}H_{15}$, 85%), 134 ([$C_{10}H_{15}$]$^+$, 44%), 119 ([C_9H_{11}]$^+$, 100%). Anal. Found: C, 58.21; H, 9.23; N, 7.80. Calc. for $C_{36}H_{66}Mo_2N_4$ (746.8): C, 57.90; H, 8.91; N, 7.50%.

3.11. Synthesis of [Re(NMes)$_3$OSiMe$_3$] (8)

Re_2O_7 (500 mg, 1.03 mmol) are dissolved in 20 ml (94.1 mmol) $(Me_3Si)_2O$ at 40 °C. To this solution 1.40 g (12.9 mmol) Me_3SiCl, 1.31 g (12.9 mmol) NEt_3 and 0.837 g (6.19 mmol) $MesNH_2$ are added and the mixture is stirred for 26 h at 45 °C. The soluble parts are separated by filtration via Celite and the solvent was stripped in vacuo. The red oily residue is dissolved with 5–10 ml pentane. At −30 °C product crystallizes. Yield: 225 mg (32%), orange–red solid, m.p. 45 °C (dec.). ^{1}H-NMR (400 MHz, C_6H_6-d_6): 0.34 (s, 9H), 2.12 (s, 9H), 2.38 (s, 18H), 6.72 (s, 6H) ppm. ^{13}C-NMR (100 MHz, C_6H_6-d_6): $\delta = 153.5$, 134.9, 131.7, 128.4, 20.9, 18.7, 2.03 ppm. IR (Nujol): 1605 w, 1463 vs, br, 1377 s, 1326 s, 1290 s, 1260 vw, 1249 m, 1163 w, 1013 w, 988 w, 888 s, br, 849 s, 837 m, 796 vw, 748 w, 720 m, 388 w cm^{-1}. Anal. Found: C, 53.71; H 6.14; N 6.15. Calc. for $C_{30}H_{42}N_3OReSi$ (675.0): C, 53.39; H, 6.27; N, 6.23%.

3.12. Synthesis of [Re(NMes)$_3$Cl] (9)

To a suspension of 5 g (10.3 mmol) Re_2O_7 in 200 ml CH_2Cl_2 at 0 °C are added successively 8.37 g (61.9 mmol) $MesNH_2$, 14.6 g (144.5 mmol) NEt_3 and 17.9 g (165.2 mmol) Me_3SiCl. The reaction mixture is stirred at 25 °C for 3 days. After all volatiles have been removed, the residue is extracted into toluene, insoluble material is separated by filtration, toluene is completely removed in vacuo and the dark red solid still containing NMR signals which are attributed to a [Re–OSiMe$_3$] group is again stirred with 8 ml Me_3SiCl at r.t. for 24 h. Finally removal of all volatiles at 10^{-3} mbar leads to a dark red solid, which is suspended and washed at −30 °C with pentane. Yield: 3.51 g (53%), dark red crystalline material, m.p. 157 °C. ^{1}H-NMR (400 MHz, C_6H_6-d_6): 2.09 (s, 9H), 2.34 (s, 18H), 6.65 (s, 6H) ppm. ^{13}C-NMR (100 MHz, C_6H_6-d_6): 153.6, 136.9, 132.4, 128.4, 20.9, 18.7 ppm. IR (Nujol): 1605 m, 1466 vs, br, 1378 s, 1317 m, 1287 vs, 1260 vw, 1162 vw, 1032 w, br, 989 m, 853 s, 798 w, 730 m, 720 s, 597 w, 593 w, 392 w, 361 s cm^{-1}. EIMS: $m/z = 621.1$ ([M]$^+$, 29%), 487.2 ([M]$^+$–NMes, 16%), 135.1 ($MesNH_2$, 100%). Anal. Found: C, 52.44; H, 5.72; N, 6.56. Calc. for $C_{27}H_{33}ClN_3Re$ (621.2): C, 52.21; H, 5.35; N 6.76%.

3.13. Synthesis of [Re(NMes)$_2$(μ-NMes)]$_2$ (10)

[Re(NMes)$_3$Cl] (250 mg, 0.402 mmol) are dissolved in 10 ml THF. At −80 °C 0.44 ml (0.443 mmol) of 1.0 M [$LiBEt_3H$] in THF. Within 1 h the solution is warmed upto r.t. where it is kept there for 1 h. The product separates as an orange precipitate. Precipitation is completed at 0 °C, the solids are filtered into a frite and extracted from the frite into with 20 ml toluene. All volatiles are removed in vacuo and the residue is crystallized from hot THF. Yield: 375 mg (80%) red crystals, m.p. 245 °C. ^{1}H-NMR (400 MHz, $CHCl_3$-d): 1.93 (s, 12H), 1.99 (s, 24H), 2.19 (s, 12H), 2.33 (s, 6H), 6.70 (s, 8H), 6.88 (s, 4H) ppm. ^{13}C-NMR (100 MHz, $CHCl_3$-d): 18.8, 19.3, 20.9, 22.6, 127.9, 129.3, 132.2, 133.5, 133.9, 135.4, 153.1, 157.3 ppm. IR (Nujol): 1606 m ν(C=C), 1377 m, 1341 vs, 1320 vs, 1290 s and 1227 m ν(Re=N–C), 1163 w, 1096 vw, br, 1028 w, 1015 w, 991 m, 885 s, 803 w, br, 726 m, 602 w cm^{-1}. EIMS: $m/z =$ 1171 ([M]$^+$, 36%), 1039 ([M]$^+$–NMes, 31%). Anal. Found: C, 53.75; H, 5.58; N, 6.65. Calc. for $C_{54}H_{66}N_6Re_2$ (1171.6): C, 55.36; H, 5.68; N, 7.17%.

3.14. Crystal structure determination of 10

Single crystals were obtained from THF. Compound **10** crystallizes in the monoclinic space group $P2_1/n$ (No. 11) with $a = 14.655(1)$, $b = 9.776(1)$, $c = 21.097(3)$ Å, $\alpha = \gamma = 90°$, $\beta = 105.978(7)°$, $V = 2905.7(4)$ Å^3, $Z = 4$. A crystal with the dimensions $0.3 \times 0.2 \times 0.1$ mm^3 was used. Intensity data were measured at 213 K with a Enraf–Nonius CAD4 (Mo–K_α radiation, $\lambda = 0.70930$ Å) upto $T_{max} = 29°$, yielding 7849 unique reflections, of which 6011 were observed. The absorption coefficient was 4.209 mm^{-1}, no absorption correction. The structure was solved by direct methods (SHELXS-86 and SHELXS-97) [36] and refined [37] by least-squares methods based on F^2 with all reflections to $R = 0.0454$ and $wR_2 = 0.1267$; residual electron density located at the rhenium atom 2.291/−2.921 e Å^{-3}. Non-hydrogen atoms were refined anisotropically, hydrogen atoms were inserted in calculated positions. The asymmetric unit contains one molecule THF and one molecule of the complex.

4. Supplementary material

Crystallographic data (excluding structure factors) for these structures have been deposited with the Cambridge Crystallographic Data Centre as supplementary publication no. CCDC-163799 (**2**), CCDC-163646 (**4a**), CCDC-163798 (**5a**), and CCDC-163797 (**10**). Copies of the data can be obtained, free of charge, on application to The Director, CCDC, 12 Union Road, Cambridge CB2 1EZ, UK (Fax: +44-1223-336033 or e-mail: deposit@ccdc.cam.ac.uk).

Acknowledgements

We gratefully acknowledge support of this work by the Deutsche Forschungsgemeinschaft (SFB 347 and SFB 260) and by the Fonds der Chemischen Industrie.

References

[1] V.C. Gibson, J. Chem. Soc. Dalton Trans. (1994) 1607.
[2] D.S. Williams, M.H. Schofield, R.R. Schrock, Organometallics 12 (1993) 4560.
[3] (a) J. Sundermeyer, D. Runge, Angew. Chem. 106 (1994) 1328; (b) J. Sundermeyer, D. Runge, Angew. Chem. Int. Ed. Engl. 33 (1994) 1255.
[4] Y.W. Chao, P.M. Rodgers, D.E. Wigley, S.J. Alexander, A.L. Rheingold, J. Am. Chem. Soc. 113 (1991) 6326.
[5] S.R. Huber, T.C. Baldwin, D.E. Wigley, Organometallics 12 (1993) 91.
[6] M.T. Benson, J.C. Bryan, A.K. Burrell, T.R. Cundari, Inorg. Chem. 34 (1995) 2348.
[7] R.D. Rogers, R. Vann Bynum, J.L. Atwood, J. Am. Chem. Soc. 100 (1978) 5238.
[8] M.L.H. Green, D.M. Michaelidou, P. Mountford, A.G. Suarez, L.-L. Wong, J. Chem. Soc. Dalton Trans., (1993) 1593.
[9] A. Schorm, J. Sundermeyer, Eur. J. Inorg. Chem. (2001) 2947.
[10] U. Radius, J. Sundermeyer, K. Peters, H.G. v. Schnering, Eur. J. Inorg. Chem. (2001) 1617.
[11] A.K. Burrell, J.C. Bryan, Organometallics 11 (1992) 3501.
[12] M.L.H. Green, G. Hogarth, P.C. Konidaris, P. Mountford, J. Chem. Soc. Dalton Trans. (1990) 3781.
[13] M.L.H. Green, G. Hogarth, P.C. Konidaris, P. Mountford, J. Organomet. Chem. 394 (1990) C9–C15.
[14] A.A. Danopoulos, C.J. Longley, G. Wilkinson, B. Hussain, M.B. Hursthouse, Polyhedron 8 (1989) 2657.
[15] A.K. Burrell, D.L. Clark, P.L. Gordon, A.P. Sattelberger, J.C. Bryan, J. Am. Chem. Soc. 116 (1994) 3813.
[16] (a) A.K. Burrell, J.C. Bryan, Angew. Chem. 105 (1993) 85; (b) A.K. Burrell, J.C. Bryan, Angew. Chem. Int. Ed. Engl. 32 (1993) 94.
[17] N. Wiberg, H.-W. Häring, U. Schubert, Z. Naturforsch. 35B (1980) 599.
[18] S. Gambarotta, A. Chiesi-Villa, C. Guastini, J. Organomet. Chem. 270 (1984) C49–C52.
[19] J.H. Osborne, A.L. Rheingold, W.C. Trogler, J. Am. Chem. Soc. 107 (1985) 7945.
[20] (a) N. Wiberg, H.-W. Häring, O. Schieda, Angew. Chem. 88 (1976) 383; (b) N. Wiberg, H.-W. Häring, O. Schieda, Angew. Chem. Int. Ed. Engl. 15 (1976) 386.
[21] (a) M. Veith, Angew. Chem. 88 (1976) 384; (b) M. Veith, Angew. Chem. Int. Ed. Engl. 15 (1976) 387.
[22] N. Wiberg, H.-W. Häring, G. Huttner, P. Friedrich, Chem. Ber. 111 (1978) 2708.
[23] S. Schmidt, J. Sundermeyer, J. Organomet. Chem. 472 (1994) 127.
[24] J. Sundermeyer, Chem. Ber. 124 (1991) 1977.
[25] U. Radius, J. Sundermeyer, Chem. Ber. 125 (1992) 2183.
[26] J. Sundermeyer, U. Radius, C. Burschka, Chem. Ber. 125 (1992) 2379.
[27] N. Wiberg, H.-W. Häring, U. Schubert, Z. Naturforsch. 33B (1978) 1365.
[28] A. Schorm, Dissertation, Marburg, 1999.
[29] W.A. Nugent, Inorg. Chem. 22 (1983) 965.
[30] We cannot exclude the possibility, that the superhydride reagent may only act as electron transfer reagent.
[31] D.S. Williams, R.R. Schrock, Organometallics 12 (1993) 1148.
[32] K.F. Miller, R.A.D. Wentworth, Inorg. Chem. 18 (1979) 984.
[33] K.A. Joergensen, Inorg. Chem. 32 (1993) 1521.
[34] (a) J. Sundermeyer, D. Runge, J.S. Field, Angew. Chem. 106 (1994) 679; (b) J. Sundermeyer, D. Runge, J.S. Field, Angew. Chem. Int. Ed. Engl. 33 (1994) 678.
[35] U. Radius, J. Sundermeyer, H. Pritzkow, Chem. Ber. 127 (1994) 1827.
[36] G.M. Sheldrick, SHELXS-86, University of Göttingen (1986) and SHELXS-97, The Program for the Solution of Crystal Structures; University of Göttingen (1997), Germany.
[37] G.M. Sheldrick, SHELXL-93, University of Göttingen (1993) and SHELXL-97, The Program for the Refinement of Crystal Structures; University of Göttingen (1997), Germany.